Proceedings of ASME Turbo Expo 2016: Turbomachinery Technical Conference and Exposition
GT2016
June 13 – 17, 2016, Seoul, South Korea

GT2016-57590

INFLUENCE OF TURBULENCE MODELLING TO CONDENSING STEAM FLOW IN THE 3D LOW-PRESSURE STEAM TURBINE STAGE

Yogini Patel*
Laboratory of Fluid Dynamics
School of Energy Systems
Lappeenranta University of Technology
Lappeenranta, Finland
Email: yogini.patel@lut.fi

Giteshkumar Patel
Laboratory of Fluid Dynamics
School of Energy Systems
Lappeenranta University of Technology
Lappeenranta, Finland
Email: giteshkumar.patel@lut.fi

Teemu Turunen-Saaresti
Laboratory of Fluid Dynamics
School of Energy Systems
Lappeenranta University of Technology
Lappeenranta, Finland
Email: teemu.turunen-saaresti@lut.fi

ABSTRACT

With the tremendous role played by steam turbines in power generation cycle, it is essential to understand the flow field of condensing steam flow in a steam turbine to design an energy efficient turbine because condensation at low pressure (LP) turbine introduces extra losses, and erosion in turbine blades. The turbulence has a leading role in condensing phenomena which involve a rapid change of mass, momentum and heat transfer. The paper presents the influence of turbulence modelling on non-equilibrium condensing steam flows in a LP steam turbine stage adopting CFD code. The simulations were conducted using the Eulerian-Eulerian approach, based on Reynolds-averaged Navier-Stokes equations coupled with a two equation turbulence model, which is included with nucleation and droplet growth model for the liquid phase. The SST k-ω model was modified, and the modifications were implemented in the CFD code. First, the performance of the modified model is validated with nozzles and turbine cascade cases. The effect of turbulence modelling on the wet-steam properties and the loss mechanism for the 3D stator-rotor stage is discussed. The presented results show that an accurate computational prediction of condensing steam flow requires the turbulence to be modelled accurately.

Nomenclature

h_{lv}	specific enthalpy (J kg^{-1})
H	total enthalpy(J kg^{-1})
I	nucleation rate (m^{-3} s^{-1})
M	mass generation rate (kg m^{-3} s^{-1})
M_m	droplet mass (kg)
P	pressure(Pa)
r	radius (m)
r_*	critical radius (m)
R	gas constant (J kg^{-1} K^{-1})
S_d	mass source term (kg m^{-2} s^{-1})
S_E	energy source term (W m^{-3})
$S_{F,m}$	momentum source term (kg m^{-2} s^{-2})
t	time (s)
T	temperature (K)
u	velocity component (m s^{-1})

Greek Letters

α	phase volume fraction
Γ_E	thermal diffusion coefficient (W m^{-1} K^{-1})
η	number of liquid droplets per unit volume (m^{-3})
μ	dynamic viscosity ($kg/m \cdot s$)
ρ	density (kg m^{-3})
σ	liquid surface tension (N m^{-1})
τ	viscous stress tensor (Pa)
τ_p	droplet response time (s)

*Corresponding author

Subscript

d	droplet index
i, j	cartesian tensor notation
l	liquid phase
v	vapour phase
x	cartesian coordinate
$0, 1, 2$	total, inlet, outlet conditions

1 INTRODUCTION

Today, steam turbines play an important role in the global power production. Thus, the advancement and understanding of technologies relevant to enhancing the general performance of steam turbines is important in order to meet the global electricity demand. However, due to the comparatively low efficiency of low pressure (LP) turbine stages, the research concerning LP stages is of special importance for the scientific community, steam turbine vendors and power plant owners. Particularly, in penultimate stages of LP turbine, the temperature of superheated vapour decreases due to rapid expansion and a condensation process takes place shortly after the state path crosses the vapour-saturation line. The expansion process causes the superheated dry steam to first subcool and then nucleate to form a two-phase mixture of saturated vapour and fine liquid droplets which is generally known as wet-steam. The presence of the liquid phase within the turbine causes irreversible thermodynamic losses, aerodynamic losses and mechanical losses or erosion. For more than a century, extensive studies of condensing steam flows have been executed by numerous researchers experimentally, theoretically and numerically. However, the experimental facilities for wet-steam flows are in short supply throughout the world. Additionally, the precise measuring of essential parameters (e.g., droplet size and its distribution, wetness fraction, etc) of these flows is very challenging and, therefore, the numerical simulations of the condensing steam flows are the most feasible option.

Turbine flows involve very intricate flow phenomena including flow transition, flow separation and mixing due to stator-rotor interaction, and turbulence is involved in all these phenomena. Moreover, the role of turbulence in wet-steam flows is significant in the processes of phase change, momentum and heat transport either at main flow regions or in boundary layers on the solid walls, particularly on the possible deposition of condensed liquid droplets. Consequently, it is essential to simulate turbulence in wet-steam flow precisely, as the ignorance of turbulence modelling to condensing steam flow calculation may cause an erroneous appraisal of key phenomena and eventually result in the modelling of erroneous losses.

In recent years, 3D numerical modelling of wet-steam flow across LP turbine including multistage blade rows has become feasible because of immense improvement in computational power for computational fluid dynamics (CFD) calculations. Nevertheless, in literature the work regarding 3D steady/unsteady CFD simulations is rather sparse. A few works e.g., [1] and [2], exists, in which CFD simulations on condensing steam flows through multistage stator-rotor cascade channels of a LP steam turbine with non-equilibrium and equilibrium condensations are presented. [3] presented numerical results of wet-steam flow with a three stage LP steam turbine test rig, in which the effect of different theoretical models for nucleation and droplet growth were examined. Further, the effect of droplet size on the deposition characteristics of the last stage stator blade and also the effect of inter-phase friction on flow field were studied by [4]. However, reported work concerning the influence of turbulence on the condensing steam flow at 3D turbine stage/stages is not available. Only few publications are available e.g., [5] and [6] in which authors conducted an analysis of turbulence modelling influence to wet-steam flow considering 2D nozzles and stator turbine cascade.

This work is the continuation of the previous works. In previous studies of [7], the influence of turbulence modelling to 2D nozzle and stator cascade flows was analyzed. Also, its corresponding influence on loss mechanism was presented. In the present work, the numerical investigation of turbulence modelling effect on condensation phenomena is extended to 3D stator-rotor stage. For this purpose, only steady state simulations were performed using a mixing plane as interface between stator and rotor domain by neglecting the interaction between the stator wakes and the rotor blade. The Eulerian-Eulerian approach has been used to model two-phase flow. In this work, the performance of modified shear-stress transport (SST) k-ω turbulence model is demonstrated with the SST k-ω turbulence model. The significance of turbulence modelling on the loss mechanism in 3D stator-rotor stage is discussed as well.

2 NUMERICAL METHODOLOGY

In this paper, all the presented results were obtained by means of the ANSYS CFX. The real gas properties were evaluated from the IAPWS-IF97 formulation in which the thermodynamic properties of steam in the subcooled region were calculated by means of extrapolations from the superheated region.

2.1 Governing equations

The mass conservation equations for vapour and liquid phases are written as follows, respectively,

$$\frac{\partial}{\partial t}(\rho_v \alpha_v) + \frac{\partial}{\partial x_j}(\rho_v \alpha_v u_{j_v}) = -\sum_{\mathrm{d}=1}^{\mathrm{D}} \mathrm{S_d} - \sum_{\mathrm{d}=1}^{\mathrm{D}} m^* \alpha_v \mathrm{I}_d, \quad (1)$$

$$\frac{\partial}{\partial t}(\rho_l \alpha_l) + \frac{\partial}{\partial x_j}(\rho_l \alpha_l u_{j_l}) = \sum_{d=1}^{D} S_d + \sum_{d=1}^{D} m^* \alpha_v I_d. \quad (2)$$

Here, m^* is the mass of stable nucleus. To estimate liquid phase, a separate equation was used to calculate droplet numbers which can be written as

$$\frac{\partial}{\partial t}(\rho_l \eta) + \frac{\partial}{\partial x_j}(\rho_l \eta u_{j_l}) = \rho_l \alpha_v I_l. \quad (3)$$

In an LP turbine, more than 90% of the total mass concentration of the liquid phase consists of a very large number of very fine droplets having sub-micron size [8]. However, due to the negligible drag effect of liquid droplets on vapour phase it could be considered that all the phases flow at the identical velocity field. Therefore, in this work, only one momentum equation was used. The momentum equation of vapour phase was based on the Reynolds-averaged Navier-Stokes (RANS) equations which can be written as

$$\frac{\partial}{\partial t}(\rho_v \alpha_v u_{i_v}) + \frac{\partial}{\partial x_j}(\rho_v \alpha_v u_{i_v} u_{j_v}) = -\alpha_v \frac{\partial P}{\partial x_i} + \frac{\partial}{\partial x_j}(\alpha_v \tau_{ij_v}) + S_{F,m}. \quad (4)$$

The energy conservation equation for the vapour phase was written as

$$\frac{\partial}{\partial t}(\rho_v \alpha_v H_v) + \frac{\partial}{\partial x_j}(\rho_v \alpha_v u_{j_v} H_v) = -\alpha_v \frac{\partial P}{\partial t} + \frac{\partial}{\partial x_j}\left(\alpha_v \Gamma_E \frac{\partial T_v}{\partial x_j}\right) + \frac{\partial}{\partial x_j}(\alpha_v u_{i_v} \tau_{ij_v}) + S_E, \quad (5)$$

More details pertaining to the governing equations and their source terms can be found in [9].

2.2 Nucleation and droplet growth model

The phase change phenomenon in condensing steam flow involves two main processes viz., nucleation and droplet growth. In this work, the nucleation rate was obtained from the classical theory of non-isothermal homogeneous condensation given by [10] which can be written as,

$$I = \frac{q_c}{(1+\theta)}\left(\frac{\rho_v^2}{\rho_l}\right)\sqrt{\frac{2\sigma}{M_m^3 \pi}} e^{-\left(\frac{4\pi r_*^2 \sigma}{3K_b T}\right)}. \quad (6)$$

Here, q_c is a condensation coefficient, K_b is the Boltzmann's constant and θ is the non-isothermal correction factor which has been adopted from [11]. The droplet growth rate equation of [12] was utilised and can be expressed as,

$$\frac{dr}{dt} = \frac{k_v}{r(1+cK_n)} \cdot \frac{(T_l - T_v)}{(h_v - h_l)\rho_l}, \quad (7)$$

where, K_n is the Knudsen number, c is the empirical factor, which is 3.18, and k_v is the thermal conductivity. More details on droplet growth rate can be found in [9].

2.3 Turbulence models

In the present work, the SST k-ω turbulence model was employed for modelling the flow turbulence. Due to the very small sizes of droplets in the vapour phase, the direct effect of liquid droplets on the flow turbulence was not considered. However, an indirect influence exists though the velocity field introduced to the turbulence models. Particulary, the vapour phase turbulence could influence the dispersion of the liquid droplets. Due to the relatively small mass concentrations and sizes of droplets, the turbulence equations were calculated for the mixture of the vapour and liquid phases. The transport equations for the turbulent kinetic energy, k, and its specific rate of dissipation, ω, can be written as [13],

$$\frac{\partial}{\partial t}(\rho k) + \frac{\partial}{\partial x_j}(\rho u_j k) = \frac{\partial}{\partial x_j}\left[\left(\mu + \frac{\mu_t}{\sigma_k}\right)\frac{\partial k}{\partial x_j}\right] + P_k - \acute{\beta}\rho k\omega + P_{kb} + S_k, \quad (8)$$

$$\frac{\partial}{\partial t}(\rho \omega) + \frac{\partial}{\partial x_j}(\rho u_j \omega) = \frac{\partial}{\partial x_j}\left[\left(\mu + \frac{\mu_t}{\sigma_\omega}\right)\frac{\partial \omega}{\partial x_j}\right] + \alpha\frac{\omega}{k}P_k - \beta\rho\omega^2 + P_{\omega b} + S_\omega. \quad (9)$$

Here, P_k indicates the production rate of turbulence due to viscous forces, P_{kb} and $P_{k\omega}$ represent the buoyancy turbulence terms for k and ω equations, respectively. The model constants were considered as: $\alpha = \frac{5}{9}$, $\beta = 0.075$, $\acute{\beta} = 0.09$, $\sigma_k = 2$, and $\sigma_\omega = 2$. The turbulent viscosity, μ_t, is defined in the SST k-ω turbulence model as

$$\mu_t = \frac{a_1 \rho k}{max(a_1 \omega, SF_2)}, \quad (10)$$

where a_1 is the model constant, S is the strain rate magnitude and F_2 is the blending functions. In this work, the SST k-ω turbulence model was modified in the manner described in the previous work of [7]. The SST k-ω turbulence model was modified

to include the modulation of turbulence kinetic energy due to liquid droplets via source terms (i.e., S_k and S_ω in Eqs. (8) and (9), respectively). Therefore, the added source terms introduce an extra turbulent kinetic energy and its dissipation to the flow via the acceleration/deceleration of the droplets. These modifications directly influence on turbulent viscosity and Reynolds stresses. In such a way momentum and energy transport equations will be affected. Furthermore, the definition of μ_t was modified by means of an expansion procedure for resolving implicit algebraic equations for the Reynolds stress tensor in terms of mean velocity gradients. The modified turbulent viscosity term including turbulence production to dissipation ratio can be written as

$$\mu_t = \frac{a_1 \rho k}{max(a_1\omega, SF_2)} \frac{C1}{C1 + \left[\frac{P_k}{\omega\beta^* k - 1}\right]}, \qquad (11)$$

where C_1 defines the Rotta return-to-isentropy approximation of the pressure-strain correlation. Here S_k represents the addition of turbulent kinetic energy including the effect of liquid mass generation and droplet response time which can be expressed as $S_k = \frac{4M}{\tau_p}(1 - f_u)k$, where f_u indicates the coefficient of droplet response to the fluid velocity fluctuations. The term S_ω can be written as $S_\omega = C_2\omega\beta^* S_k$, where C_2 and β^* are the model constants. More details about model constants and corresponding closer relations of these modification are discussed in [7]. The abovementioned modifications were implemented by the authors within the CFD code using user defined subroutines.

3 COMPUTATIONAL GRID AND NUMERICAL DETAILS

To study the influence of turbulence modelling on condensing steam flow in a LP turbine, a 3D stator-rotor stage was used. The used stator vane is the stator cascade of White [14]. However, the utilised rotor blade is not that of a real turbine geometry. It was intended to be representative of 25% of reaction for rotor at mid span. The stator blade row consisted of 30 blades while the rotor blade row included 31 blades. The blade height of stator and rotor outlet was 76 mm and 126.5 mm, respectively. However, for the sake of simplicity, both blade profiles had constant radial thickness without twisting. Moreover, the domain was modelled without rotor tip clearance in order to exclude the influence of tip swirls on the flow. The flow inlet condition was set as: $P_0 = 40300$ Pa, $T_0 = 354$ K which are the similar inlet flow conditions as of [14]. Only single passage of stator and rotor was modelled employing a periodic boundary condition in the circumferential direction. An adiabatic no-slip wall boundary was defined at the blade surfaces and at the domain walls. The computational grid is displayed in Figure 1. The grid quality/density near solid boundaries is very important to precisely resolve boundary layers. Therefore, the grid distribution near the solid surfaces was fine enough to achieve sufficiently smaller y^+

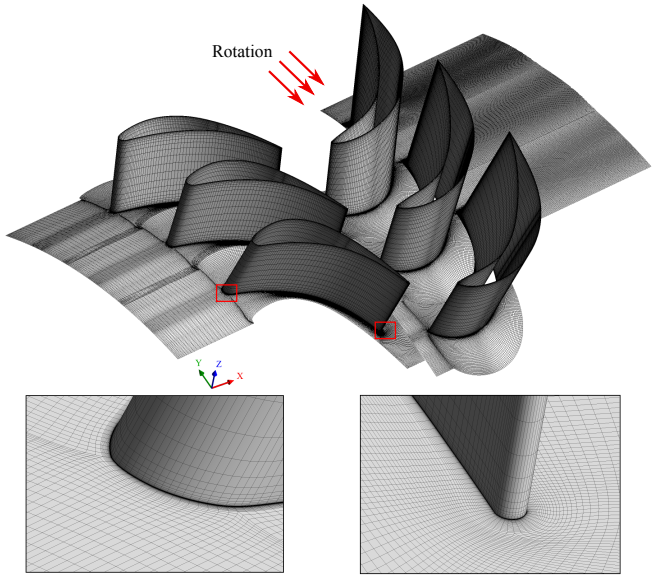

Figure 1. The computational grid.

value i.e y^+_{stator} = 3.5 and y^+_{rotor} = 2.5. An O-grid was generated near to the blade surfaces with boundary layers meshing. Moreover, the grid was more refined around the leading and trailing edges of the stator and rotor blades. Based on the previous experiences of the conducted grid independence study for 2D stator cascade case, an adequate grid refinement was assumed for this case. The computational grid included about 2.87 million hexahedral cells. All the simulations were based on finite-volume discretization and the solution of the RANS equations was done with a coupled solver. The advection was treated with high resolution scheme. Furthermore, flow turbulence models, volume fraction and energy equations were calculated using high resolution methodology. An automatic wall treatment was utilised, which provides an automatic switching from a low-Reynolds number formulation to a wall function treatment based on grid spacing near to the wall surfaces.

4 RESULTS AND DISCUSSIONS

Firstly, the performance of SST k-ω and modified SST k-ω (MSST k-ω) turbulence models were examined with the nozzle cases of [15] and [16], and also with the steam turbine stator cascade case of [14]. In Figure 2, it can be seen that both models predicted accurate pressure distributions, and the location and magnitude of the condensation shock, and yielded good correspondence with the experiments for both nozzles. Furthermore, the agreement between the predicted and the measured mean droplet radius size at the specified exit location is reasonably good for the Nozzle A of [15] for both models. However, some variation has been observed for the [16] nozzle case.

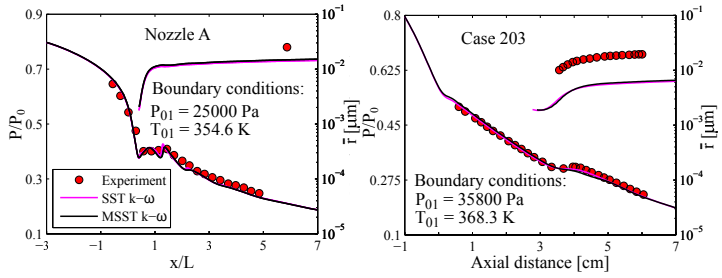

Figure 2. Comparison between the predicted and the measured data of [15] (left) and [16] (right).

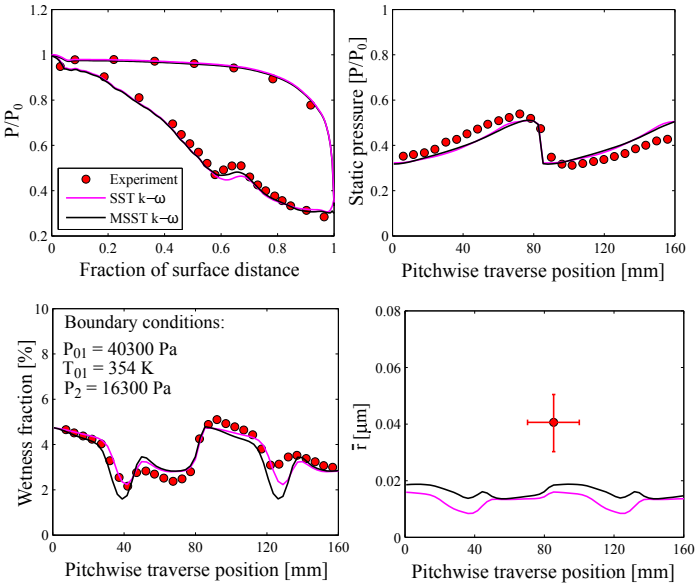

Figure 3. Comparison between the predicted and the measured data of [14] for the L1 case.

Further, the low inlet superheat experimental case named L1 of [14] has been modelled. The comparison between the predicted results of the SST k-ω model, the MSST k-ω model and the measured data is shown in Figure 3. The traverse plane is situated at the position of one fourth axial chord length from the trailing edge in axial flow direction. It can be seen that both models yielded correct trends of pressure distribution on blade surfaces. However, the MSST k-ω model estimated the correct location and intensity of the condensation disturbance on the suction side compared to the SST k-ω model. The predicted trends of static pressure and wetness fraction at traverse plane by both models are in good agreement with the experiments. Nevertheless, some discrepancy has been noted for mean droplet radius prediction.

It is fact that the flow in LP turbine has a strong three-dimensional nature due to the arrangements of stator and rotor

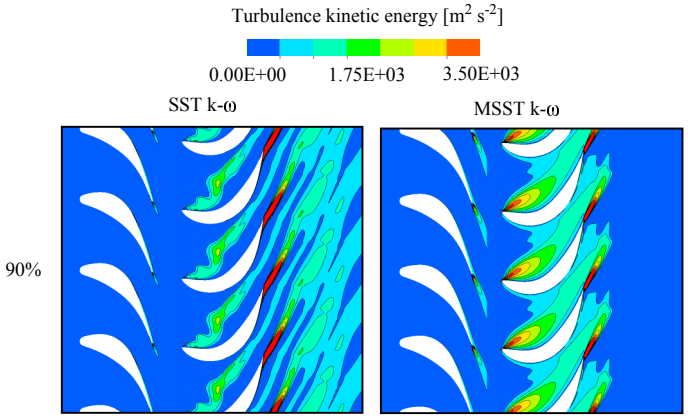

Figure 4. Predicted contours of the turbulence kinetic energy at 90% span.

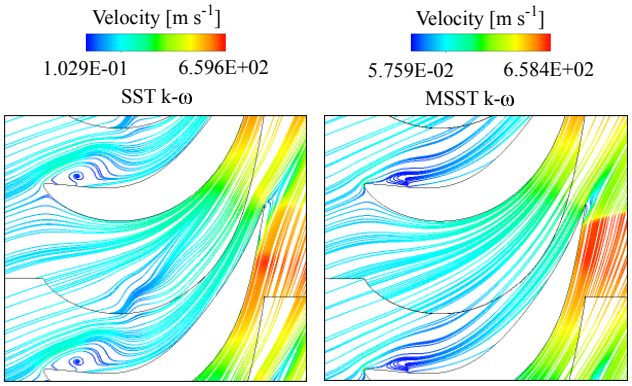

Figure 5. Predicted contours of the streamlines at 90% span.

blade rows. Moreover, the stator-rotor interaction strongly influences the flow phenomena. The wakes of stator blades enter the succeeding rotor blades, in which the flow is accelerated and rotated. Therefore, the accurate computational prediction of LP turbine flows requires the turbulence to be accurately modelled. Firstly, the influence of turbulence modelling has been analyzed with the turbulence properties. Figure 4 presents the contours of turbulence kinetic energy yielded by both models at 90% span. It is obvious that the maximum turbulent kinetic energy appears in the wake of the blades. The MSST k-ω model predicted lower turbulent kinetic energy, particularly in the wake and at the downstream of rotor blade than the SST k-ω model. This is resulted due to the viscosity modification and the effects of the added source terms, which increase the viscous dissipation considerably for the MSST k-ω model case. Moreover, the rotor blade has been generated with high curvature and therefore, the flow deflection is higher at the leading edge of the pressure side of rotor blade. Due to that a separation bubble has been observed at rotor pressure side for 90% span (Figure 5) which contributes

to the turbulent kinetic energy in the mid passage of the rotor. The MSST k-ω model estimated comparatively higher turbulent kinetic energy in the mid passage of the rotor.

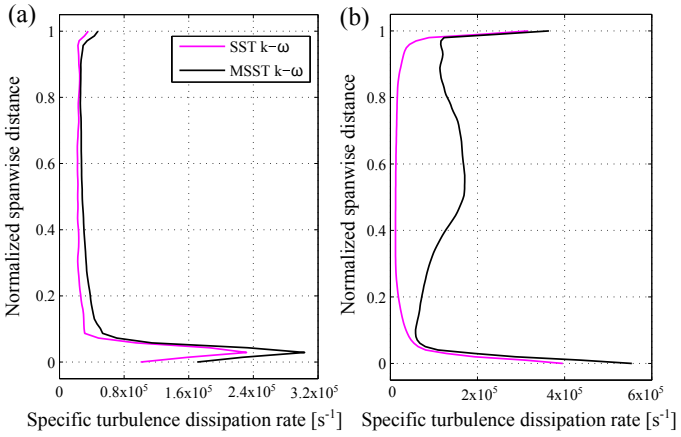

Figure 6. Predicted profiles of the specific turbulence dissipation rate at normalized spanwise distance (a) at the stator exit, and (b) outlet.

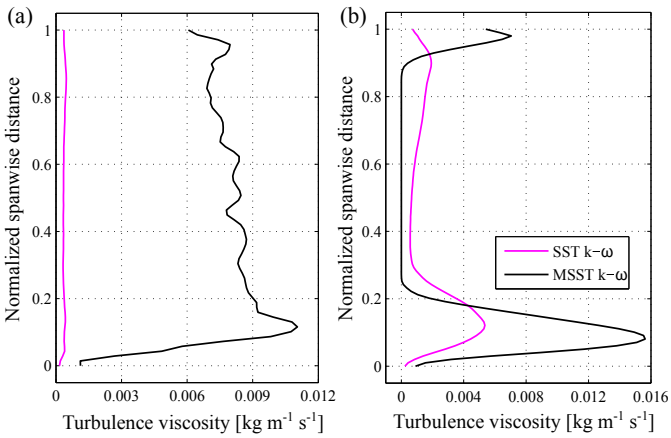

Figure 7. Predicted profiles of the turbulent viscosity at normalized spanwise distance (a) at the stator exit, and (b) outlet.

The turbomachinary flows are categorised as the wall-bounded flows in which fluid viscosity plays an important role in transport phenomena, particularly near wall surfaces. Also, the rapid variation of flow variables occurs within the boundary layer regions. These flows consist of a spectrum of different scales (eddy sizes). These structures are deformed and stretched by the fluid dynamics. These eddy structures break into smaller eddies. This phenomenon continues until the energy is transported to smaller and smaller structures. However, at the end, the kinetic energy is dissipated by the viscosity of the fluid. The whole process of transport of energy from the large scale of injection to the small dissipative scale, through the hierarchy of eddies is known as the turbulent cascade. Therefore, it is worthwhile to examine the effect of model modification on turbulence properties which are responsible for taking into account above mentioned turbulent process. The predicted circumferential average profiles of specific turbulence dissipation rate and turbulent viscosity for both the models are displayed in Figures 6 and 7. The stator exit is at the 20% axial chord distance of stator blade from the trailing edge of stator blade. It can be seen that the specific turbulence dissipation rate is notably high near the hub surface due to boundary layer effect. At outlet, the rate of specific turbulence dissipation is significantly higher at hub and shroud surfaces due to the turbulent cascade process. The MSST k-ω model yielded a higher value of specific turbulence dissipation rate at both planes than the SST k-ω model. Further, the MSST k-ω model estimated higher turbulent viscosity than the SST k-ω model. This is likely due to the modified viscosity which contains the production to dissipation ratio. Particularly, the turbulent viscosity is maximum near hub and shroud surfaces for outlet plane.

The expansion rates at stator and rotor blades, particularly at the spanwise direction, are distinct from each other. In Figure 8, the contours of vapour temperature are displayed for both models. Some variation has been observed in temperature profiles at both planes after model modification, particularly at the throat region and the downstream of it, around trailing edge and in the wake regions of rotor blade. It is obvious that the flow temperature is higher in the blade wakes due to flow mixing. In the case of MSST k-ω model, the increased viscous dissipation influenced the temperature distribution via energy source, which affected the heat transfer rates. Therefore, the temperature level is higher for the MSST k-ω model than the SST k-ω model in rotor blade wakes.

In condensing steam flow, the nucleating and growth processes are quite sensitive to local pressure distribution and expansion rate. Figure 9 shows the contours of the flow expansion rate for both models. The expansion rate varies in the blade passage, in which it is very low at the entrance and extremely high in the vicinity of the throat. As a consequence, the zone of rapid condensation occurs downstream of the throat region. As discussed previously, the rate of viscous dissipation is higher for the MSST k-ω model. Consequently, the Reynolds stresses are lower due to lesser eddy viscosity. Therefore, the shear effect is minor which influences on the flow parameters in the MSST k-ω model. Hence, the flow expansion in the MSST k-ω model is higher than the SST k-ω model.

The nucleation rate is especially large near the suction surface and at the trailing edge of the pressure surface in blade. This

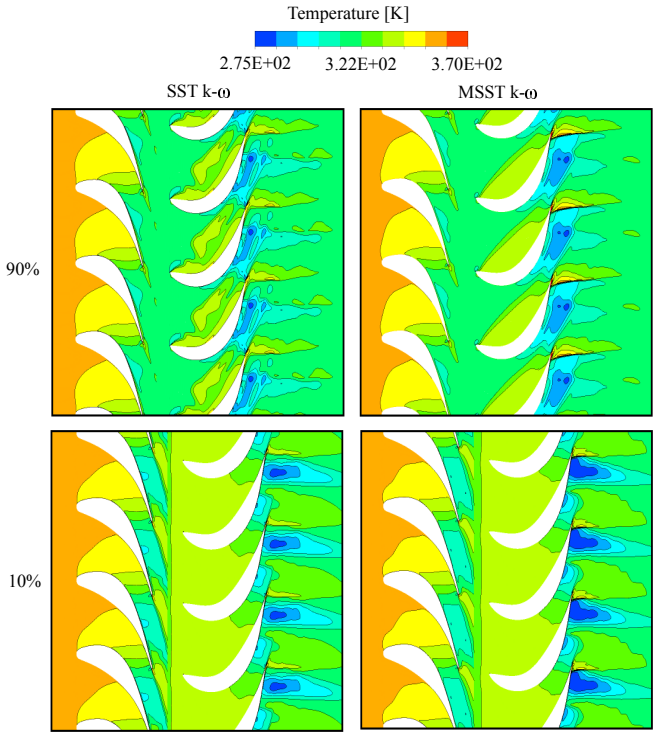

Figure 8. Predicted contours of the vapour temperature at spanwise planes.

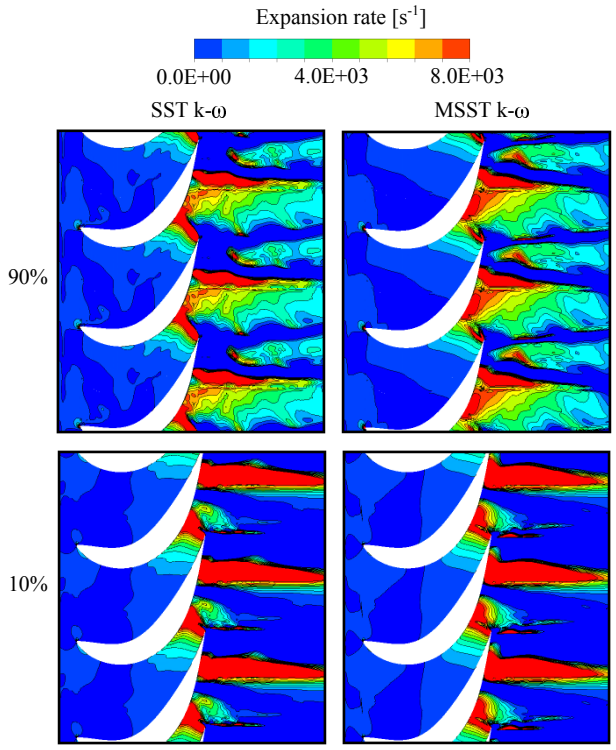

Figure 9. Predicted contours of the flow expansion rate of rotor at spanwise planes.

is caused by rapid acceleration and consequent high subcooling. The contours of subcooling and nucleation rate for both models are presented in Figures 10 and 11. The results show that the critical conditions for wetness formation have been accomplished near the hub surface for the stator within the throat region where the flow becomes transonic. The level of subcooling was reduced from the hub to the shroud surfaces for stator. While for rotor blade passage the level of subcooling was decreased from the shroud to the hub surfaces. The highest subcooling level reached was 36 K. However, some differences have been observed between the models. The MSST k-ω model estimated a higher subcooling level than the SST k-ω model. The intensity of nucleation is weaker from the hub to the shroud surfaces of stator. In addition, the nucleation region at 90% span is more uniformly distributed at rotor inlet. However, the nucleation is zeroed at the downstream of the interface at 10% and 50% span due to mixing plane assumption. The MSST k-ω model yielded a wider nucleation region than the SST k-ω model. Moreover, the expansion process is extended slightly to the downstream due to the turbulent viscosity modification and the source terms addition. Therefore, the nucleation region for the MSST k-ω model has been shifted slightly towards the downstream. Also, the level of subcooling was not strong enough to attain thermal equilibrium, and consequently the secondary nucleation zone appeared

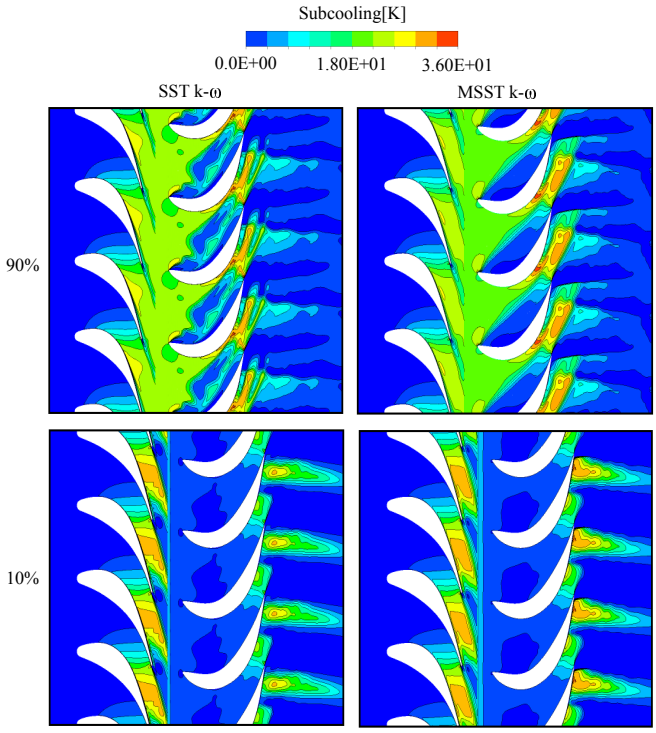

Figure 10. Predicted contours of the subcooling at spanwise planes.

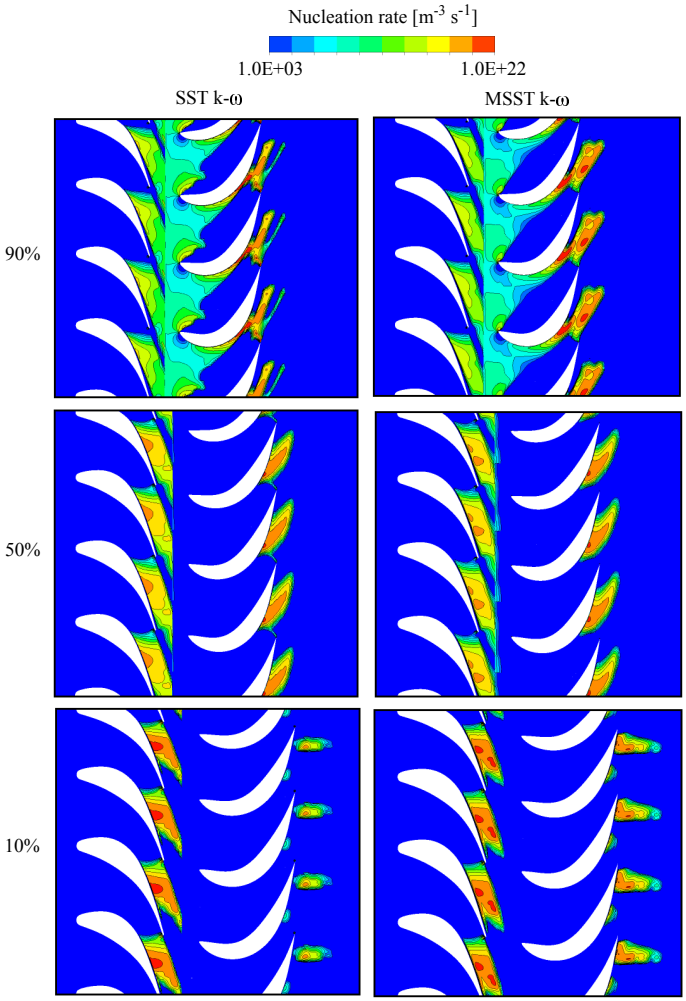

Figure 11. Predicted contours of the nucleation rate at spanwise planes.

in the rotor passage for all radial planes in both models. The intensity of secondary nucleation was decreased from the shroud to the hub surfaces of rotor for both the cases. The Wilson point fluctuates due to wake-chopping in the LP turbine flow. In the steady state calculations of this work, the secondary nucleation is stronger. This could be explained by the fixed Wilson point. The secondary nucleation region was larger for the MSST k-ω model than the SST k-ω model.

Further, the predicted contours of droplet average radius for both models at spanwise surfaces are displayed in Figure 12. If a large number of tiny liquid droplets nucleate, their growth is lower. In contrast, when a lower nucleation results, the growth rate is predominant and larger droplets are present. It can be seen that the droplet radius near the hub surface is lower due to large number of droplet. A larger droplet average radius has been observed near shroud surface. The turbulence modelling influenced the droplet sizes. The droplet radius distribution across the passage is mostly dependent on the total number of droplets created during the nucleation process, which is influenced by the distinct expansion rates along the blade passage and also the interaction between the trailing edge shock waves and the nucleation zone. It can be observed that, the growth rate is delayed in the case of MSST k-ω model due to larger nucleation region. Subsequently, the number of droplets estimated by the MSST k-ω model is lower compared to the SST k-ω model. Therefore, the MSST k-ω model yielded larger droplet average radius than the SST k-ω model.

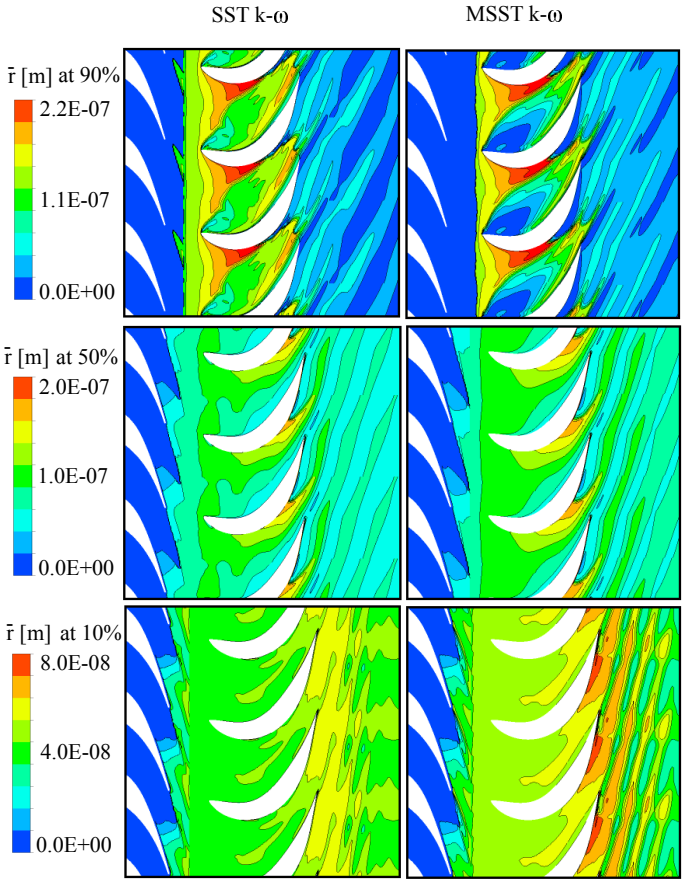

Figure 12. Predicted contours of the droplet average radius at spanwise planes.

The contours of wetness fraction are presented in Figure 13. It is clear that the level of wetness fraction increased from hub to shroud surfaces. Maximum wetness was observed in the downstream of rotor. It is clear that the SST k-ω model yielded higher wetness distribution than the MSST k-ω model. However, the MSST k-ω model predicted higher wetness fraction up to 7.5% at 90% span of rotor blade, particularly at separation bubble region of pressure side and at suction surface near trailing edge. Around

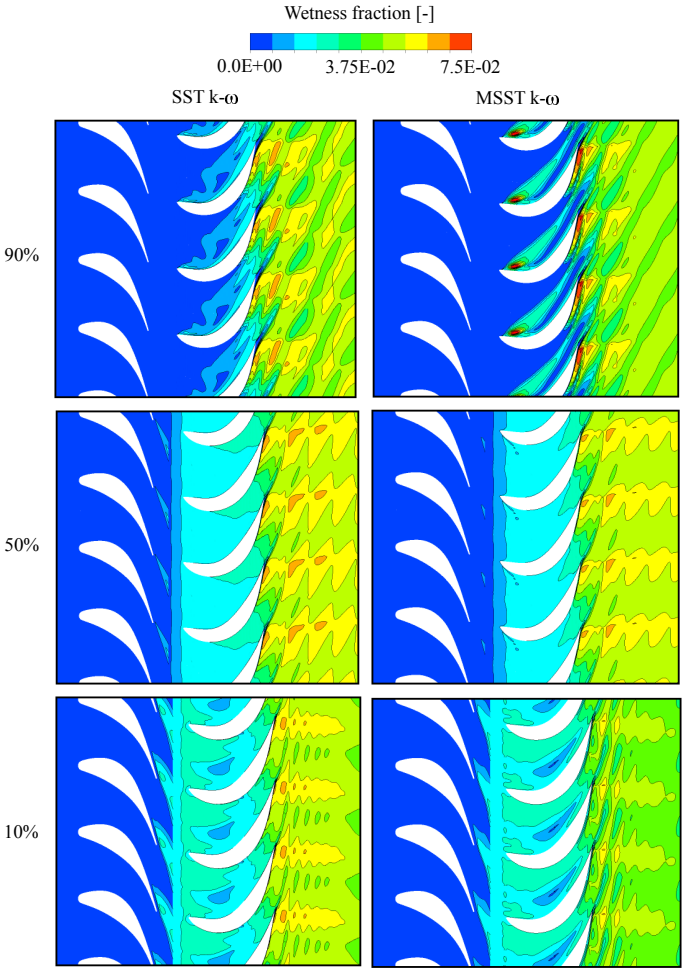

Figure 13. Predicted contours of the wetness fraction at spanwise planes.

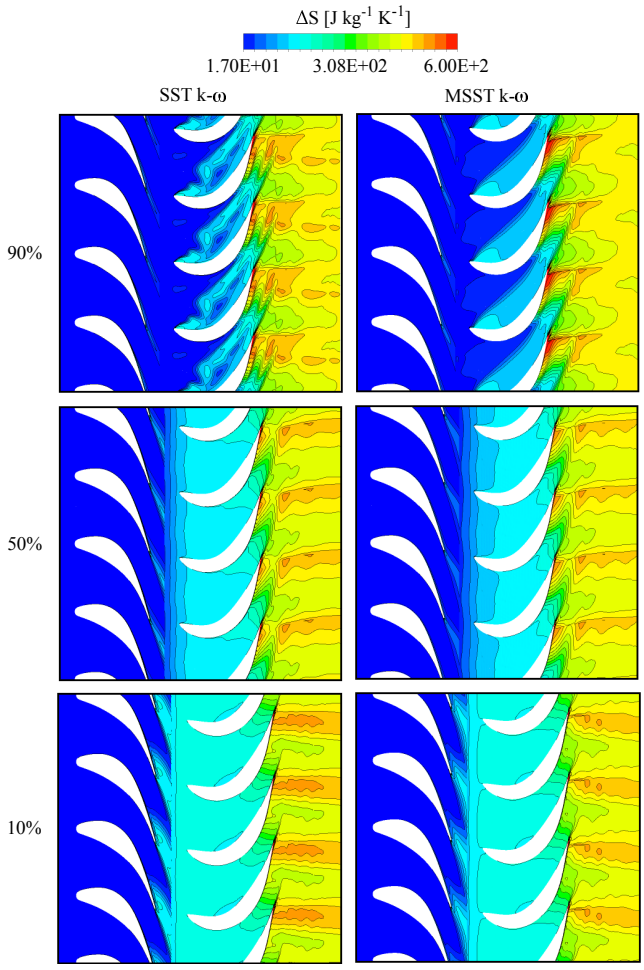

Figure 14. Predicted contours of the entropy rise at spanwise planes.

separation bubble region, the mass generation rate is considerably high which increased the wetness fraction. While at suction surface near trailing edge the wetness level is higher due to separation and secondary flow effect. Moreover, the wetness fraction is lower in the blade wakes and this is the region where flow mixing is prominent. Hence, the temperature is higher, which reduces the wetness fraction.

Figure 14 presents the predicted contours of the entropy generation for both models. Regions of steep velocity gradients such as blade wakes, edges of separated regions and vortices, in which the shear stresses are relatively high, are responsible for a large amount of entropy generation. Moreover, the flow turbulence which governs the heat, mass, and momentum transfer processes is considerably high in these regions as shown in Figure 15. It can be observed that the maximum rate of entropy is generated at the suction surface of the blade. Further, in the case of stator, the entropy generation is lower at the 90% span surface than other surfaces due to larger nucleation zone. In contrast, at the 90% span surface of the rotor, the production of entropy is raised because of very strong rotor secondary flow. However, the entropy production at the rotor is notably high compared to the stator due to the rapid release of latent heat by the droplets, flow separation and secondary flow effect. The SST k-ω model predicted a higher entropy generation compared to the MSST k-ω model particularly in the blade wake region for the 10% and 50% span surfaces, while the MSST k-ω model yielded higher entropy near to the trailing edge of rotor at the 90% span surface likely due to the higher turbulent dissipation in that region.

Further, the losses which occur due to the irreversible heat and mass transfer during the condensation process are estimated. In this work, the Markov energy loss coefficient based on the entropy increase was calculated and it can be defined as $\zeta = \frac{T_2.\Delta s}{0.5u_2^2}$, where Δs refers to the increment in a specific entropy. Here, T_2 and u_2 refer the local static temperature and relative velocity, respectively. The loss coefficient was divided into two compo-

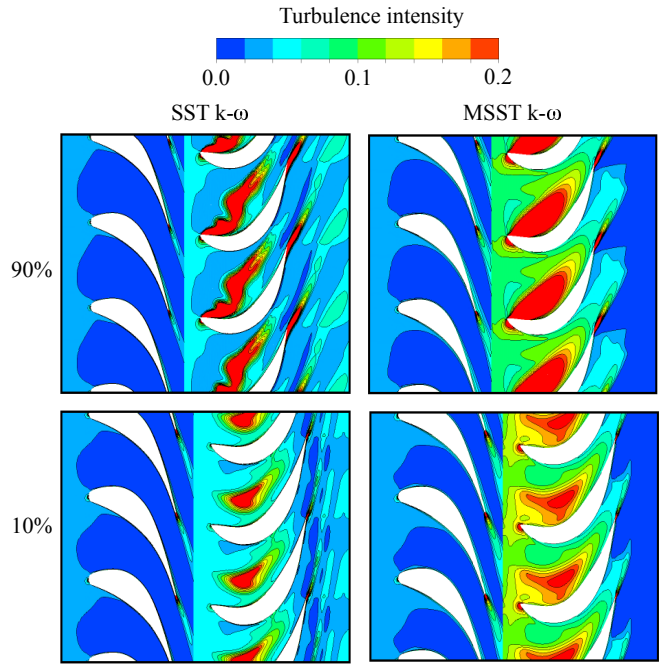

Figure 15. Predicted contours of the turbulence intensity at spanwise planes.

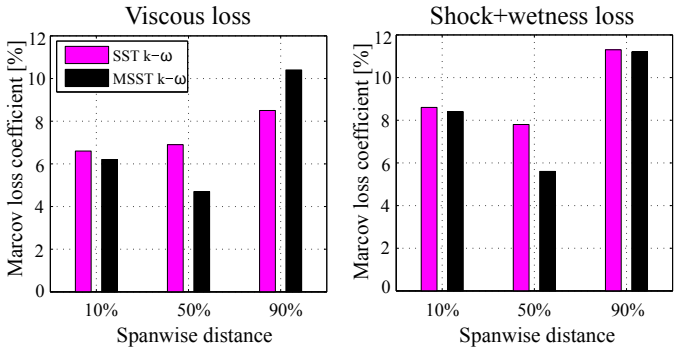

Figure 16. Predicted Markov loss coefficients.

nents: (i) shockwave plus wetness loss, which was calculated from the mass-averaged values across a section of the traverse plane excluding the wake regions, and (ii) viscous loss, which was calculated by subtracting the shockwave and wetness loss from the mass-averaged loss across the entire pitch at the traverse plane [14]. For the Markov loss coefficient estimation, all the parameters were calculated by the circumferential average at different span along the traverse plane. The traverse plane is located at the position of about 25% axial chord length from the rotor trailing edge in the axial direction. Figure 16 shows the calculated loss information. It can be seen that the SST k-ω model predicted higher viscous loss compared to the MSST k-ω model for the 10% and 50% span surfaces because of a large amount of entropy production in the blade wake of rotor (Figure 14). Moreover, it is observed that the value of viscous loss at the 90% span with the MSST k-ω was higher than with the SST k-ω model due to intense viscous dissipation at the edges of the separated region immediately behind the trailing edge of rotor. The MSST k-ω turbulence model predicted lower wetness due to higher viscous dissipation. It can be observed that the MSST k-ω model yielded lower shock plus wetness loss compared to the the SST k-ω model for all span surfaces.

5 CONCLUSIONS

The condensing steam flows at LP turbine involve rapid phase change, momentum and heat transport phenomena in which the role of turbulence is significant. Thus, the precise condensing steam flow prediction needs proper turbulence modelling. In this work, the preliminary study of the influence of turbulence modelling on non-equilibrium homogeneously condensing steam flow in 3D stator-rotor stage is discussed. For this purpose, the Eulerian-Eulerian approach based on compressible RANS equations was used. The SST k-ω turbulence model was modified by introducing the modulation of turbulence kinetic energy and its dissipation due to liquid droplets via source terms. Furthermore, the original definition of turbulent viscosity was modified by introducing production to dissipation ratio.

Firstly, the performance of MSST k-ω model was illustrated at 2D nozzles and turbine stator cascade flows. It can be concluded that the MSST k-ω model corresponded well with the test results and mimicked an accurate condensation process. The presented simulation results of a 3D stator-rotor stage case show that the inclusion of the source terms and modified turbulent viscosity at SST k-ω model caused notably higher estimates of viscous dissipation and, therefore, the increased viscous dissipation altered the temperature distribution through energy source, which impacted the heat transfer rates. Consequently, the nucleation process and droplet growth rates were influenced by the model modification. It can be seen that the MSST k-ω model yielded a higher subcooling level because of higher flow expansion. Subsequently, the nucleation region was expanded and the droplet growth rate was delayed. Therefore, the wetness fraction was decreased due to larger droplet sizes. It can be concluded that the increased viscous dissipation via model modification decreases wetness fraction.

The significance of turbulence modelling on the loss mechanism was also presented. For this purpose, the loss coefficients were estimated from the simulated results. The presented loss assessment demonstrates that after model modification the measure of shock plus wetness loss reduced. Also the viscous loss estimation was affected by the model modification and the viscous loss was decreased except near shroud surface. Based on the presented results, it is observed that the accurate computational modelling of wet-steam flow at LP turbine requires the

turbulence to be accurately modelled. Because an inaccurate prediction of turbulence may lead to an imprecise evaluation of the crucial phenomena of condensing flow and ultimately erroneous losses. However, this study is at an introductory stage in which the influence of unsteadiness is absent. Results show that the influence of turbulence modelling affected on wet-steam phenomena even with steady state simulations. Therefore, corresponding comparative simulations are encouraged concerning the further analysis of turbulence modelling influence to condensing steam flow at multistage LP turbine with unsteady condition.

ACKNOWLEDGEMENTS

The authors would like to acknowledge the Finnish Graduate School in Computational Fluid Dynamics and the Academy of Finland for the financial support and CSC-IT Center for Science, Finland for providing the scientific computing platform.

REFERENCES

[1] Yamamoto, S., Sasao, Y., Sato, S., and Sano, K., 2007. "Parallel-implicit computation of three-dimensional multistage stator-rotor cascade flows with condensation". In Proc. 18th AIAA Computational Fluid Dynamics Conference, AIAA 2007-4460, Miami, Florida, USA, June.

[2] Yamamoto, S., Sasao, Y., Kato, H., Satsuki, H., Ooyama, H., and Ishizaka, K., 2010. "Numerical and experimental investigation of unsteady 3-d wet-steam flows through two-stage stator-rotor cascade channels". In Proc. ASME Turbo Expo, GT2010-22796, Glasgow, UK, June 14-18, 1-9.

[3] Starzmann, J., Schatz, M., Casey, M. V., Mayer, J. F., and Sieverding, F., 2011. "Modelling and validation of wet steam flow in a low pressure steam turbine". In Proc. ASME Turbo Expo, GT2011-45, Vancouver, Canada, June 6-10, 1-12.

[4] Starzmann, J., Kaluza, P., Casey, M. V., and Sieverding, F., 2013. "On kinematic relaxation and deposition of water droplets in the last stages of low pressure steam turbines". *J. Turbomachinery,* **Vol. 136 (7)**, pp. 1–10.

[5] Avetissian, A. R., Philippov, G. A., and Zaichik, L. I., 2008. "Effects of turbulence and inlet moisture on two-phase spontaneously condensing flows in transonic nozzles". *Int. J. Heat Mass Transfer,* **Vol. 51**, pp. 4195–4203.

[6] Patel, Y., Patel, G., and Turunen-Saaresti, T., 2015. "Influence of turbulence modelling on non-equilibrium condensing flows in nozzle and turbine cascade". *Int. J. Heat Mass Transfer,* **Vol. 88**, pp. 165–180.

[7] Patel, Y., Turunen-Saaresti, T., Patel, G., and Grönman, A., 2014. "Numerical investigation of turbulence modelling on condensing steam flows in turbine cascade". In Proc. of ASME Turbo Expo, GT2014-26307, Düsseldorf, Germany, June 16-20, 1-14.

[8] Guha, A., 1998. "Computation, analysis and theory of two-phase flows". *The Aeronautical Journal,* **Vol.102**, pp. 71–82.

[9] Gerber, A. G., and Kermani, M. J., 2004. "A pressure based Eulerian-Eulerian multi-phase model for non-equilibrium condensation in transonic steam flow". *Int. J. Heat Mass Transfer,* **Vol. 44**, pp. 2217–2231.

[10] McDonald, J. E., 1962. "Homogeneous nucleation of vapour condensation. I -thermodynamic aspects". *Am. J. Physics,* **Vol. 30**, pp. 870–877.

[11] Kantrowitz, A., 1951. "Nucleation in very rapid vapour expansions". *J. Chem. Phys.,* **Vol.19**, pp. 1097–1100.

[12] Gyarmathy, G., 1976. *Condensation in flowing steam*. A von Karman Institute Book on Two-Phase Steam Flow in Turbines and Separators, Hemisphere, London.

[13] Menter, F. R., 1994. "Two-equation eddy-viscosity turbulence models for engineering applications". *AIAA Journal,* **Vol. 32 (8)**, pp. 1598–1605.

[14] White, A. J., Young, J. B., and Walters, P. T., 1996. "Experimental validation of condensing flow theory for a stationary cascade of steam turbine blade". *Philos. Trans. Roy. Soc. London.,* **Vol. A 354**, pp. 59–88.

[15] Moore, M. J., Walters, P. T., Crane, R. I., and Davidson, B. J., 1973. "Predicting the fog drop size in wet steam turbines". In Wet Steam 4 Conference, Institute of Mechanical Engineers (UK), University of Warwick, paper C37/73.

[16] Moses, C. A., and Stein, G. D., 1978. "On the growth of steam droplets formed in a Laval nozzle using both static pressure and light scattering measurements". *J. Fluids Eng.,* **Vol. 100**, pp. 311–322.